



Modeling orbital data of soil carbon dioxide efflux from different land uses in Southern Amazon

João Lucas Della Silva^a, Mendelson Lima^b, Larissa Pereira Ribeiro Teodoro^c,
Luís Guilherme Teixeira Crusiol^d, Newton La Scala^e, Fernando Saragosa Rossi^c, Damien Arvor^f,
Paulo Eduardo Teodoro^g, Carlos Antonio da Silva Junior^{g,*} 

^a State University of Mato Grosso (UNEMAT), PPG-BIONORTE, Sinop, 78550000, Mato Grosso, Brazil

^b State University of Mato Grosso (UNEMAT), Department of Biology, Alta Floresta, 78580000, Mato Grosso, Brazil

^c Federal University of Mato Grosso do Sul (UFMS), Chapadão do Sul, 79560000, Mato Grosso do Sul, Brazil

^d Embrapa Soja (National Soybean Research Center – Brazilian Agricultural Research Corporation), Londrina, 86001970, Paraná, Brazil

^e State University of São Paulo (UNESP), PPG-Ciência do Solo, Jaboticabal, 14884900, São Paulo, Brazil

^f Centre National de la Recherche Scientifique (CNRS), UMR 6554 LETG Université Rennes 2, Rennes, 35000, France

^g State University of Mato Grosso (UNEMAT), Department of Geography, Sinop, 78550000, Mato Grosso, Brazil

ARTICLE INFO

Keywords:

Carbon dioxide
Remote sensing
Amazon
Land use

ABSTRACT

The dynamics of carbon among atmospheric, soil and biotic stocks are of great importance for ecosystem and climate services. The interdependence of carbon stocks is volatile, since higher atmospheric CO₂ concentrations affect plant development and therefore carbon storage in terrestrial ecosystems. In addition, the carbon cycle is related to soil moisture, and sensitivity to moisture differs between ecosystems and climatic regions. In the southern Amazon, agriculture and cattle ranching activities drives anthropogenic actions and for the environmental costs. As a result, those activities impact carbon dynamics and its consequences on the environment. Modeling these dynamics in a spatialized way is possible through remote sensing images, which, together with appropriate modeling tools, allow us to understand the carbon balance at a regional level. The aim of this study is discussing the modeling of the soil carbon dioxide efflux (FCO₂) from different land uses for orbital data predictions using MODIS and PlanetScope imagery. Local data was the reference for the orbital data modeling with partial least squares regression (PLSR). Discussed models are based on soil moisture, temperature, spectral bands and also models with MODIS GPP and CO₂Flux were created. Land uses (characterized by high and low productivity soybeans, degraded pasture, productive pasture and native forest) and consisted of different subsets of inputs subsets to design PLSR equations. Results analyzes were based on the statistical metrics of linear regression (R²), mean absolute error (MAE) and root mean square error (RMSE). From those methods, it was observed that the subsets with the lowest error and highest correlation were the subsets related to soybeans. The homogeneity of soybean areas and its spectral characteristics mean greater capacity for predicting FCO₂, since the orbital images and PLSR modeling provide a higher correlation and lower error, both absolute and quadratic. On the other hand, carbon balance modeling in forest areas and pastures is limited and potentially associated with the heterogeneity of that environment.

1. Introduction

Carbon dynamics among atmospheric, soil and biotic stocks are of great importance for ecosystem and climate services (Upadhyay and Raghubanshi, 2020). Important part of total carbon budget relies on atmospheric carbon pool (Friedlingstein et al., 2022), which mostly rely on air-sea carbon uptake (Koseki et al., 2023; Rustogi et al., 2023) and

terrestrial emissions (Edenhofer et al., 2014). The interdependency of carbon stocks is volatile, since higher atmospheric concentrations of CO₂ affect the plants development, such as soybean roots system (Lessin and Ghini, 2009), leaf area, and thus, the storage of carbon in terrestrial ecosystems (Norby and Zak, 2011).

In the perspective of carbon soil emission, the microbial activity and the carbon cycle are dependent on soil moisture, and this sensitivity to

* Corresponding author.

E-mail address: carlosjr@unemat.br (C.A. Silva Junior).

<https://doi.org/10.1016/j.jsames.2024.105323>

Received 5 November 2024; Received in revised form 12 December 2024; Accepted 13 December 2024

Available online 18 December 2024

0895-9811/© 2024 Elsevier Ltd. All rights reserved, including those for text and data mining, AI training, and similar technologies.

moisture is different through ecosystems and climatic regions (Evans et al., 2022; García-Palacios and Chen, 2022). Furthermore, microbial adaptation to cyclical conditions of drought and increased soil moisture potentially implies non-linear relationships between soil moisture and respiration (Malik and Bouskill, 2022), which complex the modeling of carbon emitted by soil.

Largest part of carbon flux towards soil and biotic pools is depicted by Gross Primary Productivity (GPP), which describes from the efficiency of light use for metabolic functions and development of photosynthetic, that drive atmospheric carbon towards the biotic stock, and hence soil stock. The measurement in biophysical terms of such a metric is rather limited, and therefore, GPP estimations with remote sensing-based provides large-scale and well-set data (Welp et al., 2011). Partially based on surface reflectance of imaging sensors, orbital products are generated and made available, as seen in MODIS imagery (Running et al., 2015). From GPP, it can be observed that climate and carbon cycling fosters drought recovery (Schwalm et al., 2017).

Remotely-sensed GPP relies on sun-induced chlorophyll fluorescence and its sensitivity to water stress (Wieneke et al., 2016), what contributes to ascertain the water and carbon cycles codependency (Stein et al., 2020). GPP is made available as orbital remote sensing products due to its complexity, where only part of it is based on orbital data, as seen in MOD17A2H (Running and Zhao, 2015). The MODIS product has dependency of absorbed photosynthetically active radiation (APAR) estimations and the conversion efficiency of such radiation (ϵ), what translates the different vegetation types capability of using the sunlight to metabolic and development requirements.

Remote sensing techniques reaches carbon dynamics in different perspectives and carbon-related variables, as soil organic carbon (Angelopoulou et al., 2019), carbon monoxide (Plant et al., 2022; Zeri et al., 2011), carbon dioxide (Eldering et al., 2015; Jiang and Yung, 2019), methane (de Souza Maria et al., 2023; Zhang et al., 2021), formaldehyde (Wang et al., 2022), particulate matter (Bai et al., 2023; Kaufman et al., 1994; Yao and Henderson, 2014), CO₂Flux (Rahman et al., 2001; Souza et al., 2021) and GPP (Fernandez et al., 2021; Rossi and Santos, 2020).

Carbon models, as CO₂Flux, are closely related to land use (Della-Silva et al., 2022). In such a perspective, relating different land use and its changes to carbon makes reasonable discussion when it comes to carbon dynamics diagnoses, where the correlation among carbon stocks dynamics and land use are made by using different approaches, e.g., through physical methods of soil stocks (Nanzer et al., 2019) or remote sensing (Hui et al., 2015; Rossi et al., 2022).

Looking at southern Amazon, the land degradation due to agricultural and livestock activities sets the region importance to both anthropic actions and environmental costs (de Area Leão Pereira et al., 2020; Nepstad et al., 2008), as this leads to extreme climate conditions (Doughty et al., 2015; Reichstein et al., 2013). In turn, the atmospheric carbon uptake is reduced (Gampe et al., 2021), what lay down a feedback cycle.

The main economic activities of the region take place by using large portions of land. The agricultural activities of soybean producing are very representative in global scale, and the use of remote sensing for environmental, agronomic and economic concern are continuously carried out with surface reflectance sensors, as MODIS (Brown et al., 2007; Epiphanyo et al., 2010; Silva Junior et al., 2020).

Remote sensing imagery data processing enable the partial least squares regression (PLSR) modelling in applications on vegetation (Crusiol et al., 2021), climate (Streher et al., 2020) and carbon dynamics (Huemmerich et al., 2017) research, what was accomplished here. Such approach successfully bears datasets with more predictor variables than response variables, as seen in PLSR applied to carbon dynamics research (Castaldi et al., 2014; Žizala et al., 2019).

Since remotely-sensed data enable regional scale assessment over ecological processes and dynamics with good conditions of availability, temporality and low technical cost, modelling carbon dynamics will

provide replicable and adequate estimations of such a purpose. Then, the objective of this study was to empirically model the soil CO₂ flux at southern Amazon on different land uses by using the partial least squares regression, by using in situ and remotely-sensed spectral (spectral bands and CO₂Flux model) and product (GPP) data.

2. Materials and methods

2.1. Study site

The study was carried out on Fazenda Aurora, in Cláudia, Mato Grosso state, Brazil. There, agricultural practices and livestock rearing are developed, as well as native forest patches take place (Fig. 1), in which were defined two different classes for both soybean (C1 and C3) and pasture (C4 and C5), as well as one forest class (C2). The municipality of Cláudia is part of southern Amazon ecoregion, and have climate type as Aw (tropical climate with dry winter) according to Köppen classification (Alvares et al., 2013). Generally, the rainy period in the region starts at October and ends in April, and the dry period is from May to September.

2.2. On site data survey

In situ surveys (soil CO₂ emission, moisture and temperature) were structured in transects of 20 samples with 100 m long for each class and were built in 5 different land uses: native forest (NF), high-yield soy (HYS), low-yield soy (LYS), high-quality pasture (HQP) and low-quality pasture (LQP). The differentiation among high and low-yield soybean, as well as high and low-quality pastures, is directly related to the quantity of agricultural cycles, and therefore implies higher crop or pasture productivity. Such information was taken from the farm owner report about agricultural and livestock activities on Fazenda Aurora.

The surveys were based on soybean phenological cycle, and to grasp the whole carbon dynamics within the soybean 2020–2021 crop year, seven collections were carried out before, during the phenological cycle and after soybean harvest (Table 1).

2.2.1. Soil carbon efflux (FCO₂)

Measurements of soil CO₂ emission (FCO₂ [$\mu\text{mol m}^{-2} \text{s}^{-1}$]) were simultaneously performed in the study period, which is the soybean phenological cycle. Each class was shaped with a 20 samples-transect for each class, as mentioned. For that, two portable systems (1 system/area) were used to monitor the changes in CO₂ concentration inside the chamber using the LI-COR 8100 infrared gas analyzer (LI-COR Biosciences, 2007).

The soil chamber has an internal volume of 854.2 cm³ with a circular soil contact area at the base of 83.7 cm², which was placed on PVC collars previously inserted (24 h before the first measurement) at each sampling point to 3 cm deep, placed on bare soil over the transect. Once the chamber is calibrated (previously) and set to the measurement mode, it takes around 1.5 min to run the time-change interpolation of CO₂ concentration inside the chamber. The FCO₂ sampling was carried in conditions with no surface water sheet. Such precaution was required since the soil moisture and carbonic dynamics are deep affected by rainfall, as consequently by the water sheet size.

2.2.2. Soil moisture and temperature

Soil temperature (T_s [°C]) and soil water content, or moisture (M_s [%]), were measured simultaneously with CO₂ concentration through a temperature sensor coupled with the system, in a depth of 10 cm. M_s was registered with the reflectometer TDE Hydrosense™, (Campbell Scientific, Australia), an instrument that measures soil moisture using two 12-cm metal rods inserted perpendicularly into the soil, where soil moisture value is derived from the time it takes for an electric current to stick from a rod to another, distant 32 mm. T_s was gaged with the manual thermometer DELLT DT-625 with a single rod inserted perpendicular in soil

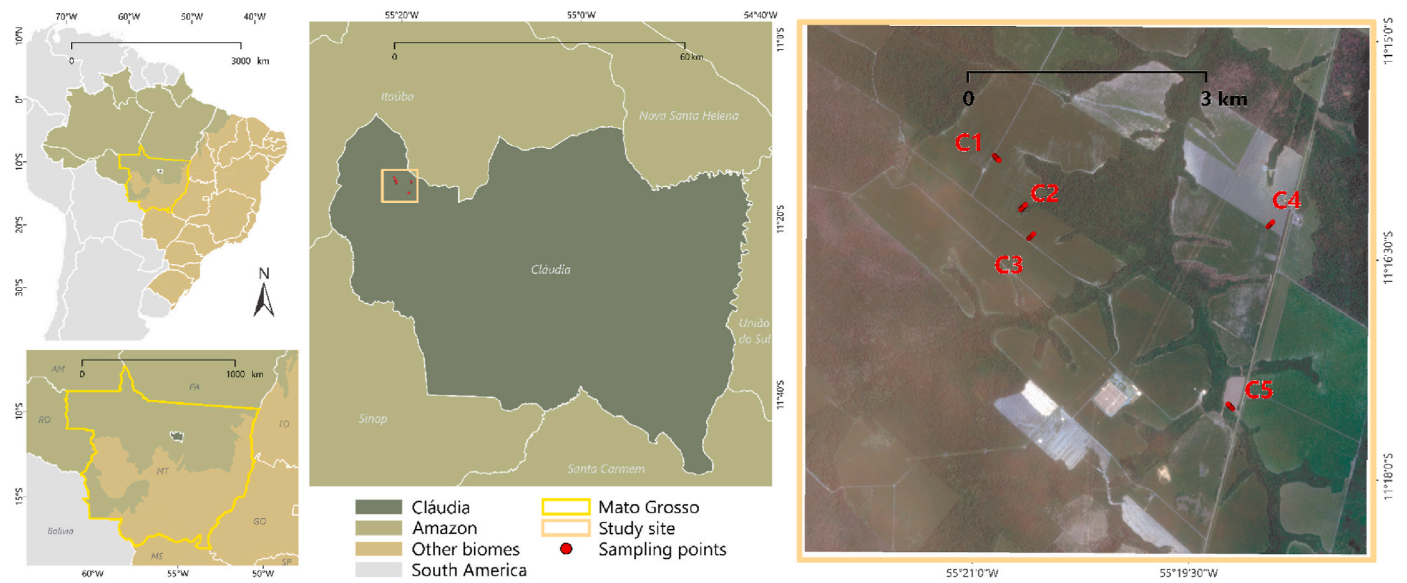


Fig. 1. Study site in Cláudia, located in southern Amazon and northern Mato Grosso state. In the municipality’s inset, the collection points are related to the different land use classes of low (C1) and high-yield (C3) soybean, forest (C2), low (C4) and high-quality (C5) pasture LULC were positioned.

Table 1
In situ data survey dates and crop season stages.

Collection date	Julian day	Crop season stage
September 26th 2020	270	Pre-sowing
October 8th 2020	282	Crop cycle
November 5th 2020	310	Crop cycle
November 26th 2020	331	Crop cycle
January 21st 2021	21	Crop cycle
March 6th 2021	65	Crop cycle
March 24th 2021	83	Postharvest

surface as well. Yet, both instruments were placed 5 cm from the PVC collars.

2.3. Remote sensing data

The surface reflectance data from orbital sensors acquired for this evaluation were based on the on-site collection dates, where the images related to the collection date were selected, if not, a date as close as possible. The selection of orbital data was limited to the visible region bands and the near infrared band, as well as looking at good conditions of cloud cover. At that step, surface reflectance from the MODIS Terra sensor systems and PlanetScope constellation were used.

PlanetScope mission offers high temporal (daily) and spatial (3 m/pixel) resolution data, and in view of availability for the dates based on four spectral bands. This imagery relies on three different sensors, what involve some different spectral traits (Table 2), but that does not affect the application with CO₂Flux data, since the spectral bands needed for this model are present throughout the PlanetScope platform.

The MOD09A1 v6.1 from MODIS data has medium temporal resolution, but with poor spatial resolution by comparing to PlanetScope. With 500 m/pixel and revisiting time of eight days, the MOD09A1 v6.1 data stands out for its historical collection of images and for its spectral characteristics (Table 3).

2.3.1. Orbital carbon dioxide flux (CO₂Flux)

The dynamics among carbon pools are mostly based on soil emission to the atmosphere, and biotic uptake from atmospheric pool towards biotic pool. Such dynamism can be expressed by CO₂Flux model (Rahman et al., 2001), where vegetation greenness and light use efficiency are represented by the normalized difference vegetation index

Table 2
PlanetScope imagery spectral bands used in this study.

Band name	Description	Spectral range (nm ^a)
Imagery from PS2		
B1	Blue	455–515
B2	Green	500–590
B3	Red	590–670
B4	NIR ^b	780–860
Imagery from PS2.SD		
B1	Blue	464–517
B2	Green	547–585
B3	Red	650–682
B4	NIR ^b	846–888
Imagery from PSB.SD		
B1	Blue	465–515
B2	Green	547–585
B3	Red	650–680
B4	NIR ^b	845–885

^a Nanometers.

^b Near infrared.

Table 3
MOD09A1.061 spectral bands used in this study.

Band name	Description	Spectral range (nm ^a)
B1	Red	620–670
B2	NIR ^b	841–876
B3	Blue	459–479
B4	Green	545–565

^a Nanometers.

^b Near infrared.

(Rouse J. W. et al., 1974) and the photochemical reflectance index (Gamon et al., 1997), respectively. In this model, the variability expressed by the NDVI and scaled PRI product is tuned by environmental traits in linear and angular coefficients, what convey the Amazon CO₂ dynamic (Santos, 2017).

$$CO_2Flux = 13.63 - 66.207 \times (sPRI \times NDVI) [\mu mol m^{-2} s^{-1}] \quad [1]$$

Where:

NDVI is the normalized difference vegetation index, given by:

$$NDVI = \frac{\rho_{NIR} - \rho_R}{\rho_{NIR} + \rho_R} \quad [2]$$

sPRI is the scaled photochemical reflectance index, given by:

$$sPRI = \frac{\frac{\rho_B - \rho_G}{\rho_B + \rho_G} + 1}{2} \quad [3]$$

Finally, for these equations:

ρ_{NIR} is the near-infrared band reflectance

ρ_R is the red band reflectance

ρ_G is the green band reflectance

ρ_B is the blue band reflectance

2.3.2. GPP

The gross primary production relies on absorbed light use efficiency by photosynthetic organisms, limited to the photosynthetically active radiation (PAR) spectra, i.e., the spectral range between 400 and 700 nm. Since only part of incident light become used for photosynthesis, the absorbed energy is namely represented by a new variable (APAR – absorber PAR), based on this efficiency (fPAR, fraction of absorbed PAR) of PAR, what is closely related to the NDVI. Yet, APAR rely also on the incident PAR (IPAR), what in turn is related to the incident shortwave radiation (SWRad). Finally, PAR related variables are coupled to the Biome Properties Look-Up Table (BPLUT – Table 4) to define the light use efficiency (ϵ). BPLUT features daily minimum temperature (TMIN) and vapor pressure deficit (VPD), what are biome related variables from MOD12 product (land cover classification).

$$GPP = \epsilon \times APAR \quad [4]$$

$$\epsilon = \epsilon_{max} \times TMIN_{scalar} \times VPD_{scalar} \quad [5]$$

$$APAR = IPAR \times FPAR \quad [6]$$

$$IPAR = SWRad \times 0.45 \quad [7]$$

MODIS GPP available as an orbital product from MODIS imagery is conditionally based on cumulative eight-day composite, spatialized on 500-m-sized pixels. Since we used the rough daily GPP and the product requires a scaling factor (given on MODIS GPP Algorithm Theoretical Basis Document - ATBD), each GPP raster was subjected to simple mathematical adjustment (Eq. (8)). The MOD17A2H product values rely on solar radiation use efficiency by photosynthetically active vegetation, both for respiration and plant growth (or namely, net primary production).

$$GPP_{actual} = \frac{GPP_{MODIS} \times 0.0001}{8} \quad [kg \ C \ m^{-2} \ d^{-1}] \quad [8]$$

Gross Primary Production.

2.4. Statistics

The data set is based on sampling at 100 points, repeated at seven different dates throughout the soybean growing cycle (2020/2021

Table 4
BPLUT parameters for GPP.

Parameter	Units	Description
ϵ_{max}	kg C MJ ⁻¹	Maximum radiation conversion efficiency
TMIN _{max}	°C	Daily minimum temperature at which $\epsilon = \epsilon_{max}$ (optimal VPD)
TMIN _{min}	°C	Daily minimum temperature at which $\epsilon = 0$ (any VPD)
VPD _{max}	Pa	Daylight average vapor pressure deficit at which $\epsilon = \epsilon_{max}$ (optimal TMIN)
VPD _{min}	Pa	Daylight average vapor pressure deficit at which $\epsilon = 0$ (any TMIN)

season). The sampling points structured five different transects of 20 sampling points on different classes of land use, being native forest, high-yield soybean, low-yield soybean, high-quality pasture and low-quality pasture. Considering the similarity between the high-yield and low-yield soybean classes, as well as between the two pasture classes, datasets combining these classes were created to be submitted to partial least squares regression (PLSR), in view of structuring the soil efflux (FCO₂) prediction based on soil moisture, temperature, GPP, CO₂Flux and the spectral bands used for those calculations.

Then, new datasets composed only of spectral bands, soil moisture and temperature data were also defined, to verify potential improved results without dependence on the GPP product and CO₂Flux. The PLSR method correlates the spectral and GPP data matrix to the soil CO₂ efflux, in view of creating a new dataset of orthogonal base vectors (latent variables or PLSR factors), which account for most of the variation in a trait variable. PLS regression modeling approach structures a linear equation consisting of each variable (spectral bands, GPP and CO₂Flux) multiplied each one by scaling coefficients.

PLSR modeling relies on splitting the dataset for calibration, k-fold cross-validation and external validation steps. For that, 70% of each subset was used as input for calibration and cross-validation (10-fold), and the remaining data based the external validation. The modelling performance was evaluated by using the determination coefficient (R²), the mean absolute error (MAE) and the root mean squared error (RMSE) between the in-situ measurements of CO₂ efflux (ground truth) and modeled CO₂ efflux from remote sensing-based data.

3. Results

Preliminary analysis of the data collected in situ makes possible to establish a prognosis of the modelling capacity of the PLSR method, besides possible limitations intrinsic to conditions of high variability and data normality. In this perspective, the difference between reference and the predicted values of FCO₂ (μmol m⁻² s⁻¹) rely on the high variability of in situ measurements, and embracing the orbital carbon variables promote similar scenarios of prediction, and therefore, error metrics (Figs. 2–9).

The partial least squares regression over the different subsets results in different equation models for one single land use classes and for three different combinations of land uses. These combined subsets were high- and low-quality pasture, and equivalently, soybean classes, as well as a final combination with the whole dataset (Tables 5 and 6). Finally, the subsets were also designed based on the orbital data source, which means that sets were based on classes or combinations of classes for the MODIS sensor data, and separately, for the PlanetScope data.

The correlation among prediction and reference most rely on the external validation subsets, but the great difference over non-normalized datasets is standardized from the calibration and cross-validation subsets (Table 7). This condition is mandatory on remote sensing data, where spatial features are affected in case of data normalization.

Considering the objective of modeling soil carbon efflux with orbital data, only external validation values were used to interpret our results. From these metrics, the limitations faced by this data set are remarkable. However, the present methodology with soybean data reached good-potential results, since this land use class had the best modelling conditions.

4. Discussion

We modeled the FCO₂ (soil CO₂ efflux) of a farming place in southern Amazon, based on partial least-squares regression and orbital data, with future outlook to put the model on regional scale, and beyond to get the impact of land uses on regional climate. The data input came from an experimental design of five transects over soybean crops, pastures and a forest, where the infrared gas analyzer instrument gauged such carbonic

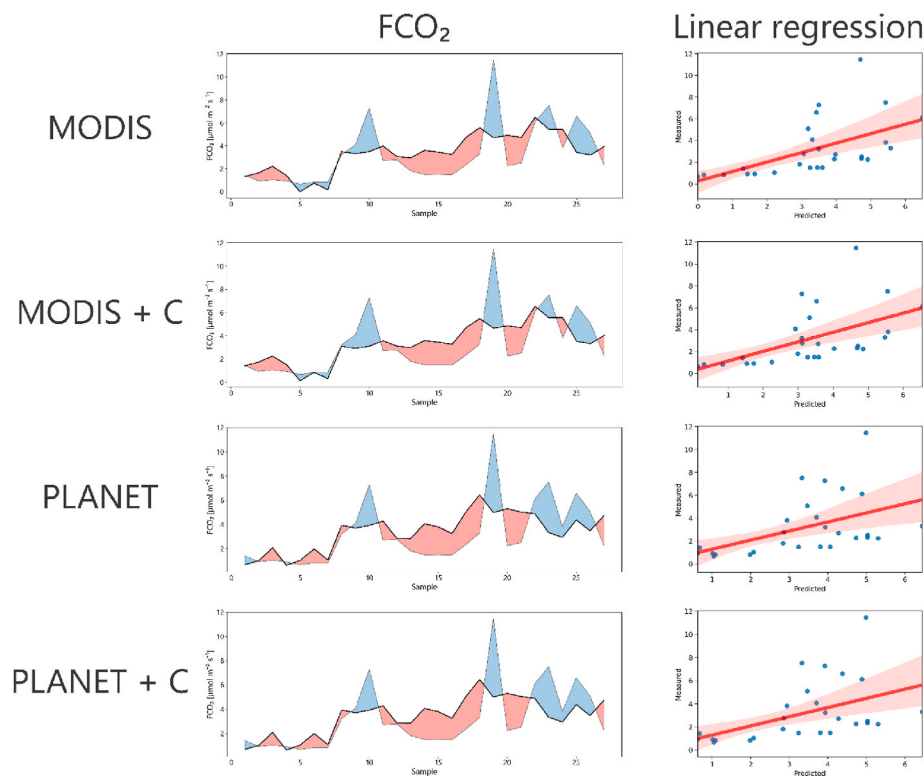


Fig. 2. Comparison between reference (grey line) and predicted (black line) FCO₂ [$\mu\text{mol m}^{-2} \text{s}^{-1}$] and the linear regression with high-yield soybean data (HYS).

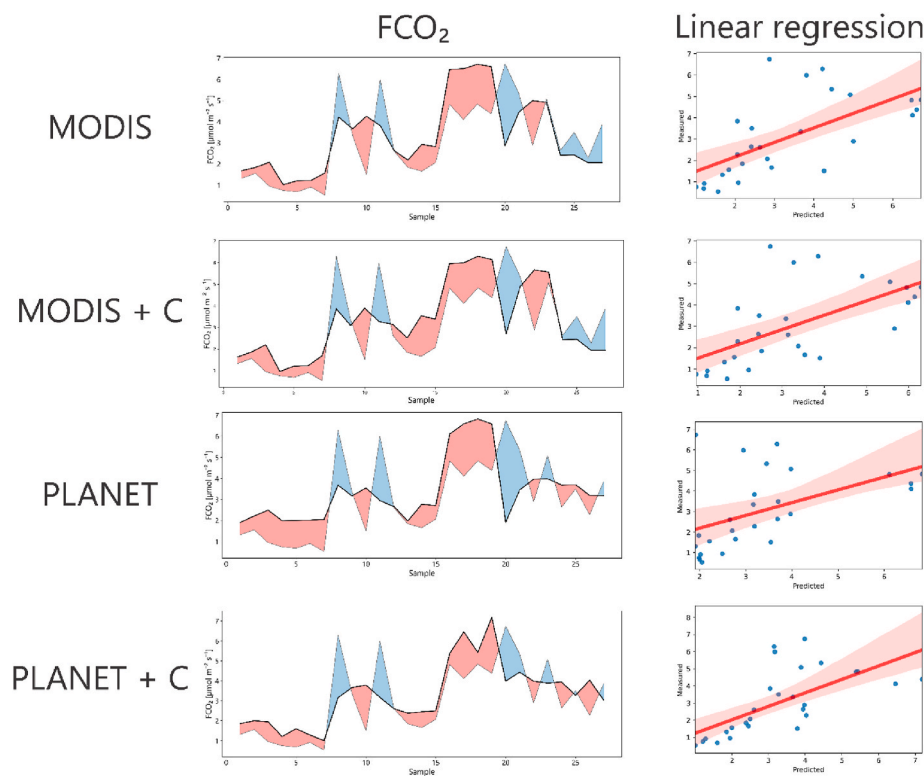


Fig. 3. Comparison between reference (grey line) and predicted (black line) FCO₂ [$\mu\text{mol m}^{-2} \text{s}^{-1}$] and the linear regression with low-yield soybean data (LYS).

metric. Despite facing limitations due to high variability and data abnormality, the impact due to soybean areas advancing over the Amazon potentially moves towards an adequate model for such task.

The soil CO₂ efflux is an important player on carbon flux from soil

towards atmospheric pool, and the close relation to land use and cover aggregates the biotic pool of carbon to this dynamism (Rossi et al., 2022, 2023). In different perspectives of PLSR modeling, carbon stocks dynamism seems very limited to reach definitive results, even more with

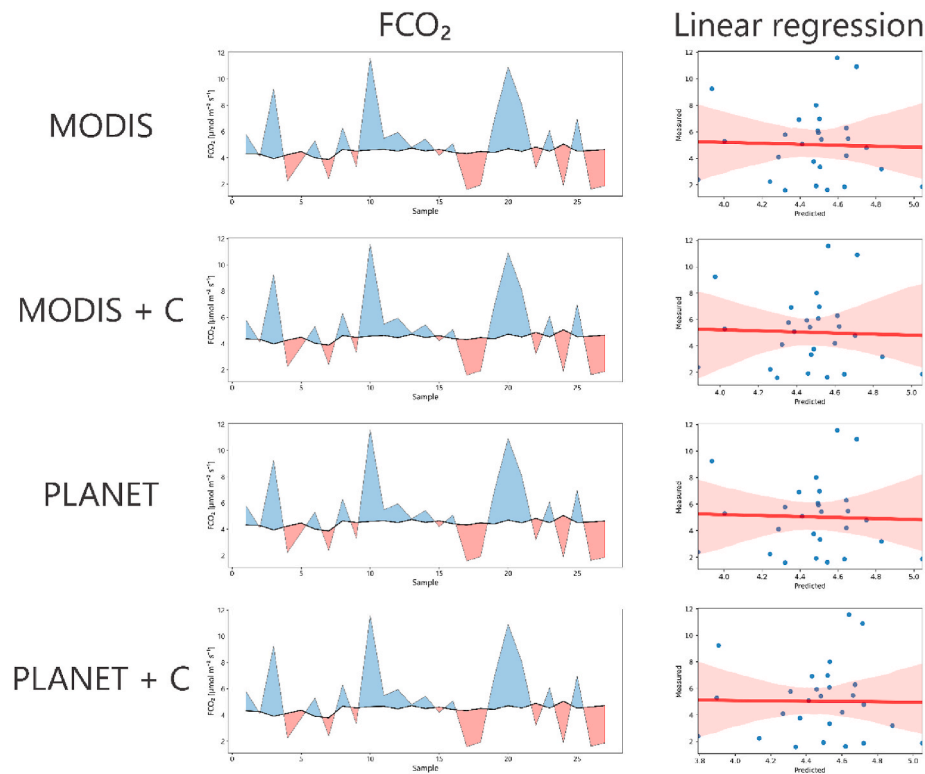


Fig. 4. Comparison between reference (grey line) and predicted (black line) FCO_2 [$\mu\text{mol m}^{-2} \text{s}^{-1}$] and the linear regression with native forest data (NF).

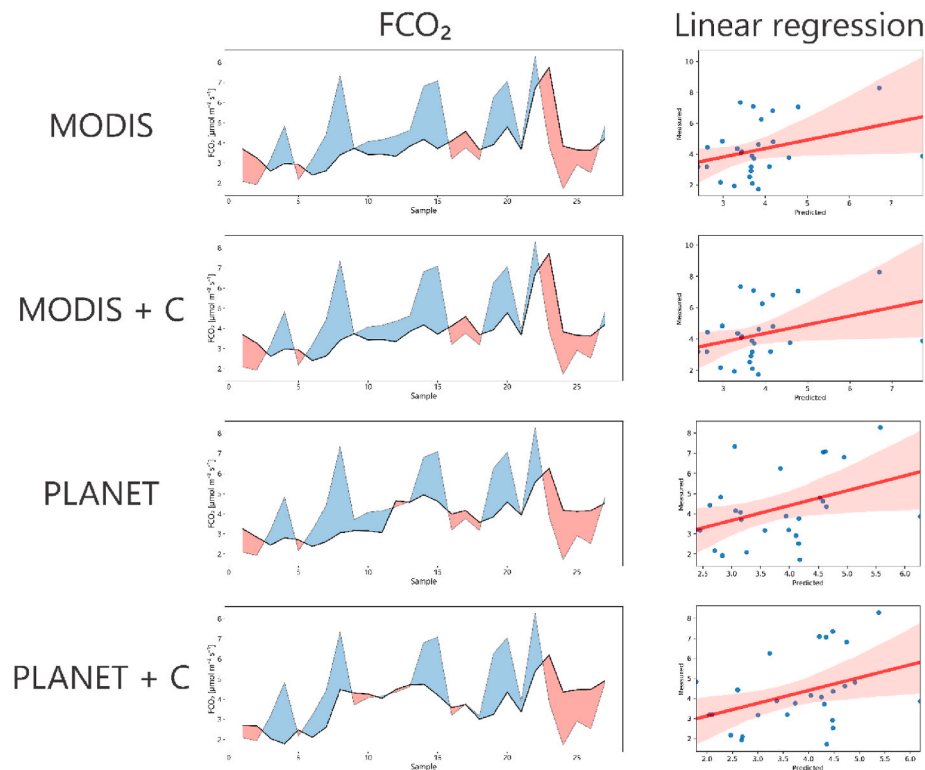


Fig. 5. Comparison between reference (grey line) and predicted (black line) FCO_2 [$\mu\text{mol m}^{-2} \text{s}^{-1}$] and the linear regression with high-quality pasture data (HQP).

non-normalization step before modeling of abnormal data. The decision to forego the normalization of these data is due to the potential for applying this model on orbital imagery, so that it will then be possible to conduct a spatialized estimate based on orbital data. It also can be taken

the temporal variability being disregarded restrained the modeling, in a condition related to dataset size.

In context, the economic base of Mato Grosso and the policies around it designs the actual land use dynamism. Being a relatively recent

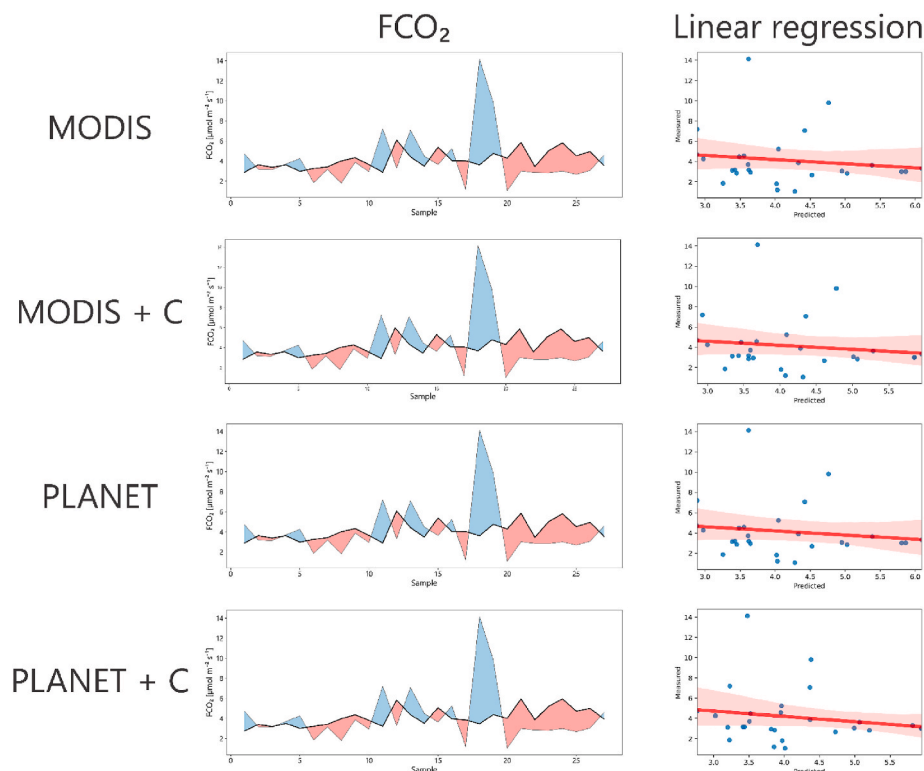


Fig. 6. Comparison between reference (grey line) and predicted (black line) FCO₂ [$\mu\text{mol m}^{-2} \text{s}^{-1}$] and the linear regression with low-quality pasture data (LQP).

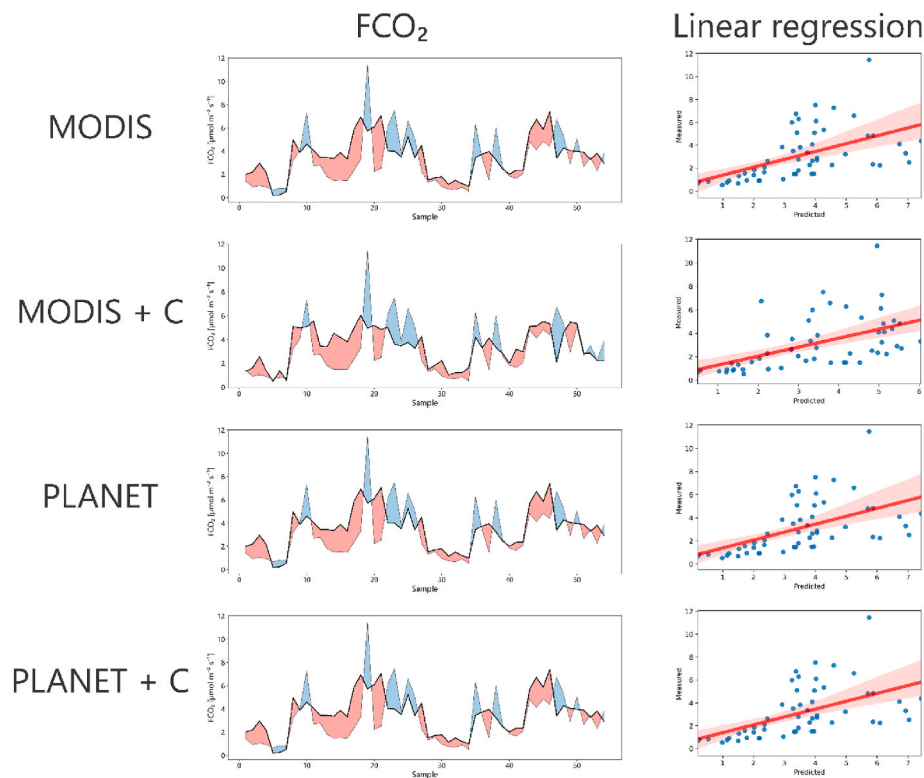


Fig. 7. Comparison between reference (grey line) and predicted (black line) FCO₂ [$\mu\text{mol m}^{-2} \text{s}^{-1}$] and the linear regression with soybean data (HYS + LYS).

occupation, the northern region of state intersects the southern region of Amazon and set the scene: replacement of native forest areas to pasture, then to agricultural lands (Gollnow et al., 2018), and sometimes, directly from forest to soybean (Barona et al., 2010). Such backdrop and

its significance foster plenty of research efforts in the convergence of remote sensing, soybean and the deforestation (Chaves and Alves, 2019; da Silva et al., 2023; Gibbs et al., 2015; Silva and Lima, 2018), as in the present work.

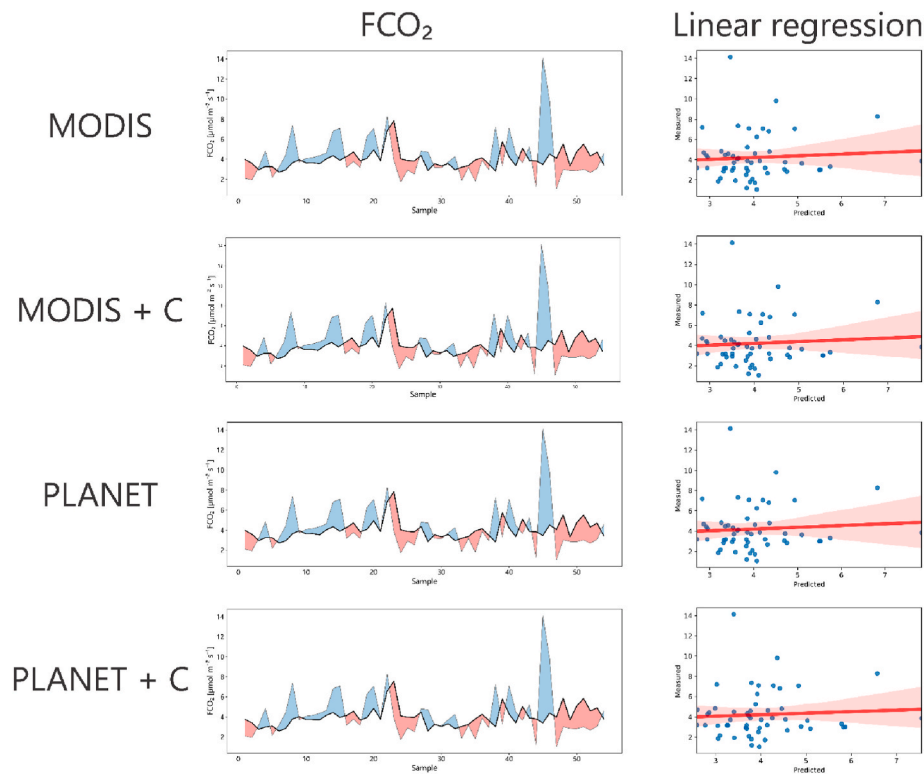


Fig. 8. Comparison between reference (grey line) and predicted (black line) FCO₂ [μmol m⁻² s⁻¹] and the linear regression with pasture data (HQP + LQP).

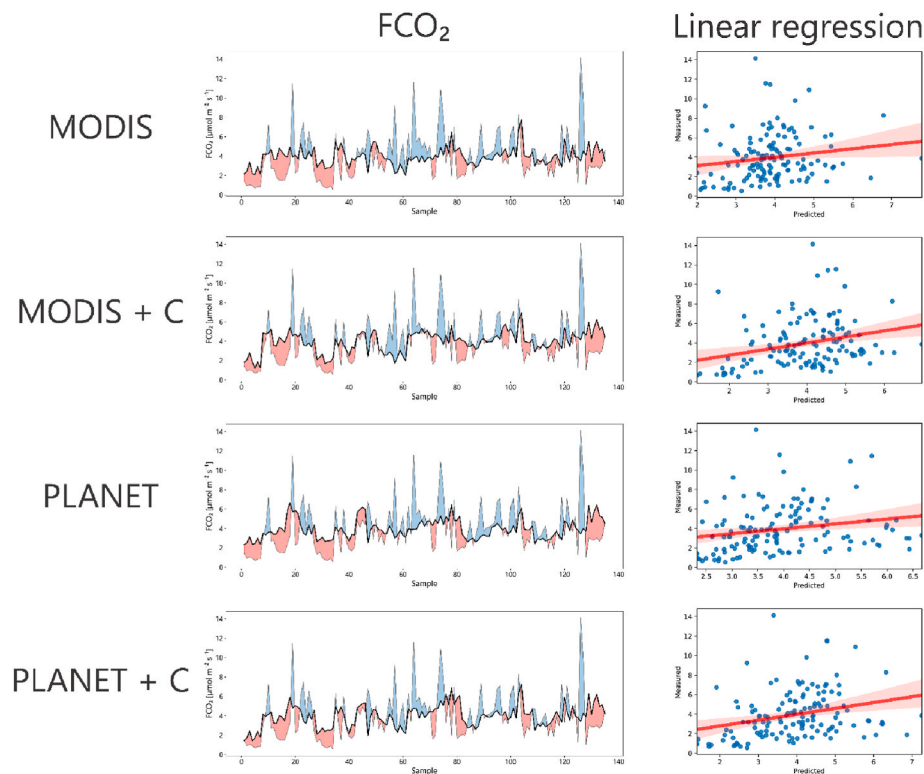


Fig. 9. Comparison between reference (grey line) and predicted (black line) FCO₂ [μmol m⁻² s⁻¹] and the linear regression with the whole dataset (ALL).

When we observe the statistical metrics of soybean results (Table 7), MODIS imagery potential is confirmed in other applications with such data: the algorithm-based approach of soybean mapping along the crop season results in accurate maps, despite of high cloud cover in the period

(Silva Junior et al., 2020). In the environmental policy concern, the effectiveness of the soy moratorium policy could be assessed with MODIS imagery, where the conversion of native forest to soybean areas (sometimes with intermediate pasture land use), the soy moratorium

Table 5

PLSR equations for soil CO₂ efflux (μmol m⁻² s⁻³) prediction with surface reflectance, soil moisture and temperature.

Imagery	Land use subset	Equation	
MODIS	HYS ^a	$FCO_2 = M_s \cdot 0.1507 + T_s \cdot 0.3056 + \rho_B \cdot (-12.78) + \rho_G \cdot (-15.29) + \rho_R \cdot (-26.37) + \rho_{NIR} \cdot (-6.03)$	
	LYS ^b	$FCO_2 = M_s \cdot 0.1211 + T_s \cdot 0.1348 + \rho_B \cdot 23.22 + \rho_G \cdot 3.60 + \rho_R \cdot (-39.19) + \rho_{NIR} \cdot 5.24$	
	HYS + LYS	$FCO_2 = M_s \cdot 0.1658 + T_s \cdot 0.1500 + \rho_B \cdot 16.21 + \rho_G \cdot 2.04 + \rho_R \cdot (-34.34) + \rho_{NIR} \cdot 2.08$	
	NF ^c	$FCO_2 = M_s \cdot 0.0573 + T_s \cdot 0.1612 + \rho_B \cdot 0.0003 + \rho_G \cdot 0.0004 + \rho_R \cdot 0.0006 + \rho_{NIR} \cdot 0.0019$	
	HQP ^d	$FCO_2 = M_s \cdot 0.2140 + T_s \cdot 0.0639 + \rho_B \cdot 8.63 \times 10^{-5} + \rho_G \cdot 0.0004 + \rho_R \cdot 0.0002 + \rho_{NIR} \cdot 0.0024$	
	LQP ^e	$FCO_2 = M_s \cdot 0.2281 + T_s \cdot 0.0732 + \rho_B \cdot (-0.0005) + \rho_G \cdot 0.0013 + \rho_R \cdot (-2.36 \times 10^{-5}) + \rho_{NIR} \cdot 0.0038$	
	HQP + LQP	$FCO_2 = M_s \cdot 0.2092 + T_s \cdot 0.0730 + \rho_B \cdot (-0.0001) + \rho_G \cdot 0.0008 + \rho_R \cdot 0.0001 + \rho_{NIR} \cdot 0.0030$	
	All ^f	$FCO_2 = M_s \cdot 0.2048 + T_s \cdot 0.0759 + \rho_B \cdot (-0.0003) + \rho_G \cdot 0.0002 + \rho_R \cdot (-0.0008) + \rho_{NIR} \cdot 0.0004$	
	Planet	HYS	$FCO_2 = M_s \cdot 0.2840 + T_s \cdot 0.0400 + \rho_B \cdot (-0.0003) + \rho_G \cdot (-0.0005) + \rho_R \cdot (-0.0022) + \rho_{NIR} \cdot 0.0048$
		LYS	$FCO_2 = M_s \cdot 0.1584 + T_s \cdot (-0.0191) + \rho_B \cdot (-0.9000) + \rho_G \cdot (-1.37) + \rho_R \cdot (-3.68) + \rho_{NIR} \cdot 9.89$
HYS + LYS		$FCO_2 = M_s \cdot 0.1901 + T_s \cdot (-0.0017) + \rho_B \cdot (-0.8267) + \rho_G \cdot (-1.22) + \rho_R \cdot (-3.42) + \rho_{NIR} \cdot 7.59$	
NF		$FCO_2 = M_s \cdot 0.0573 + T_s \cdot 0.1612 + \rho_B \cdot 0.0002 + \rho_G \cdot 0.0003 + \rho_R \cdot 0.0003 + \rho_{NIR} \cdot 0.0023$	
HQP		$FCO_2 = M_s \cdot 0.1175 + T_s \cdot (-0.0022) + \rho_B \cdot 0.7071 + \rho_G \cdot 0.8354 + \rho_R \cdot (-3.91) + \rho_{NIR} \cdot (10.62)$	
LQP		$FCO_2 = M_s \cdot 0.2281 + T_s \cdot 0.0732 + \rho_B \cdot 0.0002 + \rho_G \cdot 0.0006 + \rho_R \cdot (-0.0003) + \rho_{NIR} \cdot 0.0054$	
HQP + LQP		$FCO_2 = M_s \cdot 0.2093 + T_s \cdot 0.0730 + \rho_B \cdot 0.0004 + \rho_G \cdot 0.0007 + \rho_R \cdot 8.57 \times 10^{-5} + \rho_{NIR} \cdot 0.0038$	
All ^e		$FCO_2 = M_s \cdot 0.1300 + T_s \cdot 0.0334 + \rho_B \cdot (-0.8495) + \rho_G \cdot (-1.01) + \rho_R \cdot (-3.27) + \rho_{NIR} \cdot 7.01$	

- ^a High-yield soybean.
- ^b Low-yield soybean.
- ^c Native Forest.
- ^d High-quality pasture.
- ^e Low-quality pasture.
- ^f All classes combined.

impact on deforestation for such dynamics (Kastens et al., 2017; Silva and Lima, 2018). Our results suggest MODIS imagery and soybean occupation in the best condition of FCO₂ modeling, and supplement the high potential with soybean areas and MODIS imagery, mainly in Mato Grosso state.

Taking the mean absolute error (MAE), the native forest class present an exceptional condition where calibration present higher difference between predicted and measured FCO₂, compared to cross-validation and external validation steps. Yet, NF class also had the lowest values for R² in cross-validation and external validation, as presented the highest values of MAE in calibration and cross-validation steps. Although similar MAE results did not occur with RMSE, we emphasize that the magnitude of the error determined by the quadratic analysis means a biased estimator limitation, especially with abnormal data.

Furthermore, the heterogeneity of photosynthetic in Amazon native forest areas may affect the modeling capability of the variable predicted in this observation, potentially due to the intention of predicting biophysical values of CO₂ efflux. Such limitation is constant in modeling of carbon based on surface reflectance data, where the assessment mostly depends on different land use, as well as it is constrained to get the carbon flux variability over classes (Della-Silva et al., 2022), and the biophysical estimation of carbon dynamics in forest is constrained, when comparing to agricultural and livestock land uses, perhaps relying on the heterogeneity of this land use (Araza et al., 2023; Della-Silva et al., 2022). Future studies may consider using Amazon rainforest inventories associated to carbon dynamics metrics.

Table 6

PLSR equations for soil CO₂ efflux (μmol m⁻² s⁻¹) prediction with surface reflectance, soil temperature, soil moisture, and carbon related variables (GPP and CO₂Flux).

Imagery	Land use subset	Equation	
MODIS	HYS ^a	$FCO_2 = M_s \cdot 0.1404 + T_s \cdot 0.3110 + \rho_B \cdot (-19.74) + \rho_G \cdot (-16.61) + \rho_R \cdot (-22.65) + \rho_{NIR} \cdot (-6.95) + CO_2Flux \cdot 0.0235 + GPP \cdot 5.98$	
	LYS ^b	$FCO_2 = M_s \cdot 0.1697 + T_s \cdot 0.1763 + \rho_B \cdot (-0.0024) + \rho_G \cdot (-0.0038) + \rho_R \cdot (-0.0106) + \rho_{NIR} \cdot (0.0237) + CO_2Flux \cdot (-0.6059) + GPP \cdot 0.0056$	
	HYS + LYS	$FCO_2 = M_s \cdot 0.2053 + T_s \cdot 0.1265 + \rho_B \cdot (-0.0041) + \rho_G \cdot (-0.0048) + \rho_R \cdot (-0.01) + \rho_{NIR} \cdot (0.0132) + CO_2Flux \cdot (-0.4213) + GPP \cdot 0.0042$	
	NF ^c	$FCO_2 = M_s \cdot 0.0571 + T_s \cdot 0.1603 + \rho_B \cdot 0.0003 + \rho_G \cdot 0.0005 + \rho_R \cdot 0.0006 + \rho_{NIR} \cdot 0.0019 + CO_2Flux \cdot 0.0119 + GPP \cdot 0.0002$	
	HQP ^d	$FCO_2 = M_s \cdot 0.2131 + T_s \cdot 0.0649 + \rho_B \cdot 0.0001 + \rho_G \cdot 0.0004 + \rho_R \cdot 0.0002 + \rho_{NIR} \cdot 0.0024 + CO_2Flux \cdot (-0.0071) + GPP \cdot 0.0007$	
	LQP ^e	$FCO_2 = M_s \cdot 0.2181 + T_s \cdot 0.0806 + \rho_B \cdot (-0.0005) + \rho_G \cdot 0.0013 + \rho_R \cdot 3.87 \times 10^{-6} + \rho_{NIR} \cdot 0.0038 + CO_2Flux \cdot (-0.0504) + GPP \cdot 0.0011$	
	HQP + LQP	$FCO_2 = M_s \cdot 0.2062 + T_s \cdot 0.0761 + \rho_B \cdot (-0.00013) + \rho_G \cdot 0.00083 + \rho_R \cdot 0.00014 + \rho_{NIR} \cdot 0.00301 + CO_2Flux \cdot (-0.0246) + GPP \cdot 0.00084$	
	All ^f	$FCO_2 = M_s \cdot 0.166 + T_s \cdot 0.124 + \rho_B \cdot (-0.0011) + \rho_G \cdot 0.00012 + \rho_R \cdot (-0.0036) + \rho_{NIR} \cdot 0.0106 + CO_2Flux \cdot (-0.3069) + GPP \cdot 0.0027$	
	Planet	HYS	$FCO_2 = M_s \cdot 0.2507 + T_s \cdot 0.0682 + \rho_B \cdot (-0.0002) + \rho_G \cdot (-0.0003) + \rho_R \cdot (-0.0002) + \rho_{NIR} \cdot 0.0042 + CO_2Flux \cdot (-0.1742)$
		LYS	$FCO_2 = M_s \cdot 0.0621 + T_s \cdot 0.1263 + \rho_B \cdot 34.38 + \rho_G \cdot 25.29 + \rho_R \cdot 15.16 + \rho_{NIR} \cdot (-10.01) + CO_2Flux \cdot (-0.9803)$
HYS + LYS		$FCO_2 = M_s \cdot 0.1042 + T_s \cdot 0.1116 + \rho_B \cdot 25.27 + \rho_G \cdot 24.15 + \rho_R \cdot 13.51 + \rho_{NIR} \cdot (-8.26) + CO_2Flux \cdot (-0.9013)$	
NF		$FCO_2 = M_s \cdot 0.0567 + T_s \cdot 0.1593 + \rho_B \cdot 0.0002 + \rho_G \cdot 0.0003 + \rho_R \cdot 0.0003 + \rho_{NIR} \cdot 0.0024 + CO_2Flux \cdot (-0.0185)$	
HQP		$FCO_2 = M_s \cdot 0.1383 + T_s \cdot 0.1192 + \rho_B \cdot 0.0011 + \rho_G \cdot 0.0013 + \rho_R \cdot (-0.0015) + \rho_{NIR} \cdot 0.0084 + CO_2Flux \cdot (-0.4127)$	
LQP		$FCO_2 = M_s \cdot 0.1869 + T_s \cdot 0.0890 + \rho_B \cdot 0.0002 + \rho_G \cdot 0.0006 + \rho_R \cdot (-0.0001) + \rho_{NIR} \cdot 0.0046 + CO_2Flux \cdot (-0.0890)$	
HQP + LQP		$FCO_2 = M_s \cdot 0.1972 + T_s \cdot 0.0812 + \rho_B \cdot 0.0004 + \rho_G \cdot 0.0006 + \rho_R \cdot 0.0001 + \rho_{NIR} \cdot 0.0037 + CO_2Flux \cdot (-0.0748)$	
All		$FCO_2 = M_s \cdot 0.1810 + T_s \cdot 0.0933 + \rho_B \cdot 2.26 \times 10^{-5} + \rho_G \cdot 0.0001 + \rho_R \cdot (-0.0008) + \rho_{NIR} \cdot 0.0048 + CO_2Flux \cdot (-0.1510)$	

- ^a High-yield soybean.
- ^b Low-yield soybean.
- ^c Native Forest.
- ^d High-quality pasture.
- ^e Low-quality pasture.
- ^f All classes combined.

The low metrics in pasture related classes suggests that maintaining the same land use over time may contribute to homogeneity of pasture cover, since low quality pasture rely on a latest sowing, and still, the longer livestock raising contribute to standardizing such occupation. The similar results in HQP, LQP and then combined are related to the small difference in the spectral input data among different grazing lands (Guerschman et al., 2003). In another perspective, the different land use spectral traits that based our methods affects data compliance to PLSR modeling. Finally, and more remote, both the seasonality and the technology of genetic improvement used in soybean seeds compared to material intended for livestock farming are responsive on land use homogeneity.

Table 7

Determination coefficient (R^2), mean absolute error (MAE) and root mean squared error (RMSE) for calibration, cross-validation and external validation between ground truth measurements and prediction of CO_2 efflux ($\mu\text{mol m}^{-2} \text{s}^{-1}$) on different data subsets.

		R^2			MAE [$\mu\text{mol m}^{-2} \text{s}^{-1}$]			RMSE [$\mu\text{mol m}^{-2} \text{s}^{-1}$]		
		CA ^a	CV ^b	EV ^c	CA ^a	CV ^b	EV ^c	CA ^a	CV ^b	EV ^c
HYS	MODIS	0.4490	0.3966	0.3119	1.2590	1.3175	1.6452	1.7458	1.8302	2.1471
	MODIS + C	0.3626	0.3320	0.3003	1.3701	1.4023	1.6390	1.8124	1.8561	2.1629
	Planet	0.2135	0.1849	0.1828	1.5238	1.5523	1.7469	2.0859	2.1262	2.3398
LYS	Planet + C	0.3626	0.3320	0.2263	1.3701	1.4023	1.7836	1.8124	1.8561	2.2902
	MODIS	0.5848	0.5357	0.4162	0.9975	1.0521	1.1897	1.2980	1.3771	1.5349
	MODIS + C	0.5861	0.5357	0.3659	0.9853	1.0398	1.2487	1.2950	1.3746	1.5854
NF	Planet	0.4403	0.4026	0.2469	1.2074	1.2468	1.3882	1.5060	1.5563	1.7228
	Planet + C	0.5861	0.5357	0.4227	0.9853	1.0398	1.1426	1.2950	1.3746	1.4606
	MODIS	0.0283	0.0050	0.0012	2.0470	2.0662	1.4659	1.7426	1.7893	1.9409
HQP	MODIS + C	0.0270	0.0055	0.0014	2.0472	2.0665	1.4628	1.8699	1.9228	1.9600
	Planet	0.0283	0.0050	0.0012	2.0470	2.0662	1.6635	1.8892	1.9218	2.0858
	Planet + C	0.0270	0.0055	0.0002	2.0472	2.0665	1.5606	1.8699	1.9228	2.0077
LQP	MODIS	0.2169	0.1920	0.1190	1.1866	1.2108	1.4408	1.5132	1.5445	1.7806
	MODIS + C	0.3444	0.3041	0.1193	1.0508	1.0851	1.4417	1.3684	1.4168	1.7785
	Planet	0.2387	0.1921	0.1618	1.0877	1.1287	1.3601	1.4761	1.5318	1.6960
HYS + LYS	Planet + C	0.3444	0.3041	0.1524	1.0508	1.0851	1.3329	1.3684	1.4168	1.7351
	MODIS	0.0254	0.0137	0.0189	1.6859	1.7170	2.1274	2.1708	2.2109	2.9516
	MODIS + C	0.0312	0.0179	0.0175	1.6542	1.6854	2.1210	2.1549	2.1946	2.9428
HQP + LQP	Planet	0.0254	0.0137	0.0189	1.6859	1.7169	2.1273	2.1707	2.2108	2.9516
	Planet + C	0.0312	0.0179	0.0291	1.6542	1.6854	2.1214	2.1549	2.1946	2.9691
	MODIS	0.4106	0.3804	0.3063	1.2500	1.2821	1.4659	1.7426	1.7893	1.9409
All ^d	MODIS + C	0.3942	0.3609	0.2735	1.3207	1.3571	1.4628	1.8699	1.9228	1.9600
	Planet	0.3068	0.2826	0.1913	1.4432	1.4668	1.6635	1.8892	1.9218	2.0858
	Planet + C	0.3942	0.3609	0.2838	1.3207	1.3571	1.5606	1.8699	1.9228	2.0077
All ^d	MODIS	0.0649	0.0524	0.0051	1.5043	1.5293	1.7267	1.9945	2.0235	2.4088
	MODIS + C	0.0655	0.0574	0.0053	1.5043	1.5227	1.7287	1.9928	2.0122	2.4052
	Planet	0.0649	0.0611	0.0051	1.5043	1.5119	1.7266	1.9944	2.0026	2.4088
All ^d	Planet + C	0.0906	0.0793	0.0040	1.4579	1.4727	1.7404	1.9569	1.9762	2.4248
	MODIS	0.0568	0.0526	0.0266	1.7858	1.7923	1.8827	2.4247	2.4331	2.4787
	MODIS + C	0.1425	0.1357	0.0795	1.6459	1.6533	1.7947	2.3002	2.3106	2.3926
All ^d	Planet	0.1322	0.1227	0.0428	1.6880	1.6984	1.8967	2.3100	2.3239	2.4559
	Planet + C	0.1425	0.1357	0.0775	1.6459	1.6533	1.7952	2.3001	2.3106	2.4026

^a Calibration step.

^b Cross-validation step.

^c External validation step.

^d All classes combined.

5. Conclusion

Dioxide carbon dynamism over soil, biotic and atmospheric pools is related to several ecosystem services and climatic conditions, and the close relation to temperature and water dynamics lead us to look at such variable in view of climate change, especially in regional scale. Yet, the land use change as driver of CO_2 directly and successive affects environment, climate and finally, the mankind itself. Partial least squares regression modeling is a useful tool for such dynamics, despite the limitations of joining the whole temporal variability in a single subset and abnormal distribution of data. It was possible to confirm the soybean data from MODIS suitability to such carbon related modeling, as well as observe the limitations of spatial heterogeneity to pastures and mainly native forests remotely sensed data. The use of these models in future research work will possibly satisfactorily estimate the efflux of soil carbon dioxide for the environmental conditions of soybean agricultural areas in the southern Amazon.

CRediT authorship contribution statement

João Lucas Della Silva: Writing – review & editing, Writing – original draft, Visualization, Software, Methodology, Investigation, Formal analysis, Data curation, Conceptualization. **Mendelson Lima:** Writing – original draft, Validation, Supervision, Resources, Investigation, Conceptualization. **Larissa Pereira Ribeiro Teodoro:** Writing – review & editing, Software, Methodology, Investigation, Formal analysis, Data curation. **Luís Guilherme Teixeira Crusiol:** Writing – original draft, Software, Methodology, Formal analysis, Conceptualization.

Newton La Scala: Writing – review & editing, Visualization, Validation, Supervision, Investigation, Formal analysis, Conceptualization. **Fernando Saragosa Rossi:** Writing – original draft, Software, Methodology, Investigation, Data curation, Conceptualization. **Damien Arvor:** Writing – review & editing, Writing – original draft, Validation, Software, Methodology, Investigation, Conceptualization. **Paulo Eduardo Teodoro:** Writing – review & editing, Writing – original draft, Visualization, Validation, Software, Methodology, Formal analysis, Data curation, Conceptualization. **Carlos Antonio da Silva Junior:** Writing – review & editing, Supervision, Resources, Project administration, Methodology, Investigation, Funding acquisition, Formal analysis, Data curation, Conceptualization.

Ethical

All ethical practices have been followed in relation to the development, writing, and publication of the article entitled ORBITAL DATA MODELING OF SOIL CARBON DIOXIDE EFFLUX IN DIFFERENT USES IN SOUTHERN AMAZON.

Declaration of competing interest

The authors declare that they have no known competing financial interests or personal relationships that could have appeared to influence the work reported in this paper.

Acknowledgements

The authors would like to thank the Universidade do Estado do Mato Grosso (UNEMAT), Universidade Federal de Mato Grosso do Sul (UFMS), Centre National de la Recherche Scientifique (CNRS), Conselho Nacional de Desenvolvimento Científico e Tecnológico (CNPq) – Grant numbers 304979/2022-8, 308295/2023-4, and 309250/2021-8. The result of this research is part of the CNPq productivity scholarship project of the last author and leader of the research. It is also an experimental part of the doctoral thesis of the first author, supervised by the project leader. This study was financed in part by the Coordenação de Aperfeiçoamento de Pessoal de Nível Superior—Brazil (CAPES) – Financial Code 001.

Data availability

Data will be made available on request.

References

- Alvares, C.A., Stape, J.L., Sentelhas, P.C., Gonçalves, J.L. de M., Sparovek, G., others, 2013. Köppen's climate classification map for Brazil. *Meteorol. Z.* 22, 711–728.
- Angelopoulou, T., Tziolas, N., Balafoutis, A., Zalidis, G., Bochtis, D., 2019. Remote sensing techniques for soil organic carbon estimation: a review. *Rem. Sens.* <https://doi.org/10.3390/rs11060676>.
- Araza, A., de Bruin, S., Hein, L., Herold, M., 2023. Spatial predictions and uncertainties of forest carbon fluxes for carbon accounting. *Sci. Rep.* 13, 12704. <https://doi.org/10.1038/s41598-023-38935-8>.
- Bai, K., Li, K., Sun, Y., Wu, L., Zhang, Y., Chang, N.-B., Li, Z., 2023. Global synthesis of two decades of research on improving PM_{2.5} estimation models from remote sensing and data science perspectives. *Earth Sci. Rev.* 241, 104461. <https://doi.org/10.1016/j.earscirev.2023.104461>.
- Barona, E., Ramankutty, N., Hyman, G., Coomes, O.T., 2010. The role of pasture and soybean in deforestation of the Brazilian Amazon. *Environ. Res. Lett.* 5, 024002. <https://doi.org/10.1088/1748-9326/5/2/024002>.
- Brown, J.C., Jepson, W.E., Kastens, J.H., Wardlow, B.D., Lomas, J.M., Price, K.P., 2007. Multitemporal, Moderate-spatial-resolution remote sensing of modern agricultural production and land Modification in the Brazilian Amazon. *Gisci Remote Sens* 44, 117–148. <https://doi.org/10.2747/1548-1603.44.2.117>.
- Castaldi, F., Casa, R., Castrignanò, A., Pascucci, S., Palombo, A., Pignatti, S., 2014. Estimation of soil properties at the field scale from satellite data: a comparison between spatial and non-spatial techniques. *Eur. J. Soil Sci.* 65, 842–851. <https://doi.org/10.1111/ejss.12202>.
- Chaves, M.E.D., Alves, M. de C., 2019. Recent applications of the MODIS sensor for soybean crop monitoring and deforestation detection in Mato Grosso, Brazil. *CAB Reviews: Perspectives in Agriculture, Veterinary Science, Nutrition and Natural Resources.* <https://doi.org/10.1079/PVNSNRR201914007>.
- Crusiol, L.G.T., Nanni, M.R., Furlanetto, R.H., Sibaldelli, R.N.R., Cezar, E., Sun, L., Foloni, J.S.S., Mertz-Henning, L.M., Nepomuceno, A.L., Neumaier, N., Farias, J.R.B., 2021. Yield prediction in soybean crop Grown under different levels of water availability using reflectance spectroscopy and partial least squares regression. *Remote Sens (Basel)* 13. <https://doi.org/10.3390/rs13050977>.
- da Silva, R.F.B., Moran, E.F., Millington, J.D.A., Viña, A., Liu, J., 2023. Complex relationships between soybean trade destination and tropical deforestation. *Sci. Rep.* 13, 11254. <https://doi.org/10.1038/s41598-023-38405-1>.
- de Area Leão Pereira, E.J., de Santana Ribeiro, L.C., da Silva Freitas, L.F., de Barros Pereira, H.B., 2020. Brazilian policy and agribusiness damage the Amazon rainforest. *Land Use Pol.* 92, 104491. <https://doi.org/10.1016/j.landusepol.2020.104491>.
- de Souza Maria, L., Rossi, F.S., Costa, L.M. da, Campos, M.O., Blas, J.C.G., Panosso, A.R., Silva, J.L. Della, Silva Junior, C.A. da, La Scala, Jr N., 2023. Spatiotemporal analysis of atmospheric XCH₄ as related to fires in the Amazon biome during 2015–2020. *Remote Sens. Appl.* 30, 100967. <https://doi.org/10.1016/j.rsase.2023.100967>.
- Della-Silva, J.L., da Silva Junior, C.A., Lima, M., Teodoro, P.E., Nanni, M.R., Shiratsuchi, L.S., Teodoro, L.P., Capristo-Silva, G.F., Baio, F.H., de Oliveira, G., de Oliveira-Júnior, J.F., Rossi, F.S., 2022. CO₂Flux model assessment and comparison between an Airborne hyperspectral sensor and orbital Multispectral imagery in southern Amazonia. *Sustainability.* <https://doi.org/10.3390/su14095458>.
- Doughty, C.E., Metcalfe, D.B., Girardin, C.A.J., Amézquita, F.F., Cabrera, D.G., Huasco, W.H., Silva-Espejo, J.E., Araujo-Murakami, A., Da Costa, M.C., Rocha, W., Feldpausch, T.R., Mendoza, A.L.M., Da Costa, A.C.L., Meir, P., Phillips, O.L., Malhi, Y., 2015. Drought impact on forest carbon dynamics and fluxes in Amazonia. *Nature* 519, 78–82. <https://doi.org/10.1038/nature14213>.
- Edenhofer, Ottmar, Pichs-Madruga, Ramón, Sokona, Youba, Farahani, Ellie, Kadner, Susanne, Seyboth, Kristin, Adler, Anna, Baum, Ina, Brunner, Steffen, Eickemeier, Patrick, Kriemann, Benjamin, Savolainen, Jussi, Schlömer, Steffen, von Stechow, Christoph, Zwinkel, Timm, Minx, Jan C., 2014. *Climate Change 2014: Mitigation of Climate Change. Contribution of Working Group III to the Fifth Assessment Report of the Intergovernmental Panel on Climate Change.* Cambridge, United Kingdom and New York, NY, USA.
- Eldering, A., Pollock, R., Lee, R., Rosenberg, R., Oyafuso, F., Crisp, D., Chapsky, L., Granat, R., 2015. *Orbiting Carbon Observatory (OCO)-2 Level 1B Theoretical Basis Document.*
- Epiphonio, R.D.V., Formaggio, A.R., Rudorff, B.F.T., Maeda, E.E., Barreto Luiz, A.J., 2010. Estimating soybean crop areas using spectral-temporal surfaces derived from MODIS images in Mato Grosso, Brazil. *Pesqui. Agropecu. Bras.* 45, 72–80.
- Evans, S.E., Allison, S.D., Hawkes, C.V., 2022. Microbes, memory and moisture: predicting microbial moisture responses and their impact on carbon cycling. *Funct. Ecol.* 36, 1430–1441. <https://doi.org/10.1111/1365-2435.14034>.
- Fernandez, H.M., Granja-Martins, F.M., Pedras, C.M.G., Fernandes, P., Isidoro, J.M.G.P., 2021. An assessment of forest fires and CO₂ gross primary production from 1991 to 2019 in Mação (Portugal). *Sustainability.* <https://doi.org/10.3390/su13115816>.
- Friedlingstein, P., O'Sullivan, M., Jones, M.W., Andrew, R.M., Gregor, L., Hauck, J., Le Quéré, C., Luijckx, I.T., Olsen, A., Peters, G.P., Peters, W., Pongratz, J., Schwingshackl, C., Sitch, S., Canadell, J.G., Giais, P., Jackson, R.B., Alin, S.R., Alkama, R., Arneeth, A., Arora, V.K., Bates, N.R., Becker, M., Bellouin, N., Bittig, H.C., Bopp, L., Chevallier, F., Chini, L.P., Cronin, M., Evans, W., Falk, S., Feely, R.A., Gasser, T., Gehlen, M., Gkritzalis, T., Gloege, L., Grassi, G., Gruber, N., Gürses, Ö., Harris, I., Hefner, M., Houghton, R.A., Hurtt, G.C., Iida, Y., Ilyina, T., Jain, A.K., Jersild, A., Kadono, K., Kato, E., Kennedy, D., Klein Goldewijk, K., Knauer, J., Korsbakken, J.I., Landschützer, P., Lefèvre, N., Lindsay, K., Liu, J., Liu, Z., Marland, G., Mayot, N., McGrath, M.J., Metzl, N., Monacci, N.M., Munro, D.R., Nakaoka, S.-I., Niwa, Y., O'Brien, K., Ono, T., Palmer, P.L., Pan, N., Pierrot, D., Poccock, K., Poulter, B., Resplandy, L., Robertson, E., Rödenbeck, C., Rodriguez, C., Rosan, T.M., Schwinger, J., Séférian, R., Shutler, J.D., Skjelvan, I., Steinhoff, T., Sun, Q., Sutton, A.J., Sweeney, C., Takao, S., Tanhua, T., Tans, P.P., Tian, X., Tian, H., Tilbrook, B., Tsujino, H., Tubiello, F., van der Werf, G.R., Walker, A.P., Wanninkhof, R., Whitehead, C., Willstrand Wranne, A., Wright, R., Yuan, W., Yue, C., Yue, X., Zaehele, S., Zeng, J., Zheng, B., 2022. Global carbon budget 2022. *Earth Syst. Sci. Data* 14, 4811–4900. <https://doi.org/10.5194/essd-14-4811-2022>.
- Gamon, J.A., Serrano, L., Surfus, J.S., 1997. The photochemical reflectance index: an optical indicator of photosynthetic radiation use efficiency across species, functional types, and nutrient levels. *Oecologia* 112, 492–501. <https://doi.org/10.1007/s004420050337>.
- Gampe, D., Zscheischler, J., Reichstein, M., O'Sullivan, M., Smith, W.K., Sitch, S., Buermann, W., 2021. Increasing impact of warm droughts on northern ecosystem productivity over recent decades. *Nat Clim Chang* 11, 772–779. <https://doi.org/10.1038/s41558-021-01112-8>.
- García-Palacios, P., Chen, J., 2022. Emerging relationships among soil microbes, carbon dynamics and climate change. *Funct. Ecol.* 36, 1332–1337. <https://doi.org/10.1111/1365-2435.14028>.
- Gibbs, H.K., Rausch, L., Munger, J., Schelly, I., Morton, D.C., Noojipady, P., Soares-Filho, B., Barreto, P., Micol, L., Walker, N.F., 2015. Environment and development. Brazil's soy moratorium. *Science* 347, 377–378. <https://doi.org/10.1126/science.aaa0181>.
- Gollnow, F., Hissa, L. de B.V., Rufin, P., Lakes, T., 2018. Property-level direct and indirect deforestation for soybean production in the Amazon region of Mato Grosso, Brazil. *Land Use Pol.* 78, 377–385. <https://doi.org/10.1016/j.landusepol.2018.07.010>.
- Guerschman, J.P., Paruelo, J.M., Di Bella, C., Giallorenzi, M.C., Pacin, F., 2003. Land cover classification in the Argentine Pampas using multi-temporal Landsat TM data. *Int J Remote Sens* 24, 3381–3402. <https://doi.org/10.1080/0143116021000021288>.
- Huemrich, K.F., Campbell, P.K.E., Gao, B.-C., Flanagan, L.B., Goulden, M., 2017. ISS as a platform for optical remote sensing of ecosystem carbon fluxes: a case study using HICO. *IEEE J Sel Top Appl Earth Obs Remote Sens* 10, 4360–4375. <https://doi.org/10.1109/JSTARS.2017.2725825>.
- Hui, D., Deng, Q., Tian, H., Luo, Y., 2015. Climate change and carbon Sequestration in forest ecosystems. In: *Handbook of Climate Change Mitigation and Adaptation.* Springer, New York, pp. 1–40. https://doi.org/10.1007/978-1-4614-6431-0_13-2.
- Jiang, X., Yung, Y.L., 2019. Global patterns of carbon dioxide variability from satellite observations. *Annu. Rev. Earth Planet Sci.* 47, 225–245. <https://doi.org/10.1146/annurev-earth-053018-060447>.
- Kastens, J.H., Brown, J.C., Coutinho, A.C., Bishop, C.R., Esquerdo, J.C.D.M., 2017. Soy moratorium impacts on soybean and deforestation dynamics in Mato Grosso, Brazil. *PLoS One* 12, 1–21. <https://doi.org/10.1371/journal.pone.0176168>.
- Kaufman, Y.J., Holben, B.N., Tanré, D., Ward, D.E., 1994. Remote sensing of biomass burning in the Amazon. *Rem. Sens. Rev.* 10, 51–90. <https://doi.org/10.1080/02757259409532237>.
- Koseki, S., Tjiputra, J., Fransner, F., Crespo, L.R., Keenlyside, N.S., 2023. Disentangling the impact of Atlantic Niño on sea-air CO₂ flux. *Nat. Commun.* 14, 3649. <https://doi.org/10.1038/s41467-023-38718-9>.
- Lessin, R.C., Ghini, R., 2009. Efeito do aumento da concentração de CO₂ atmosférico sobre o oídio e o crescimento de plantas de soja. *Trop Plant Pathol* 34, 385–392. <https://doi.org/10.1590/S1982-5676200900600004>.
- LI-COR Biosciences, 2007. *LI-8100 Automated Soil CO₂ Flux System & LI-8150 Multiplexer Instruction Manual.* Lincoln.
- Malik, A.A., Bouskill, N.J., 2022. Drought impacts on microbial trait distribution and feedback to soil carbon cycling. *Funct. Ecol.* 36, 1442–1456. <https://doi.org/10.1111/1365-2435.14010>.
- Nanzer, M.C., Ensinas, S.C., Barbosa, G.F., Barreta, P.G.V., de Oliveira, T.P., da Silva, J.R. M., Paulino, L.A., 2019. Total organic carbon stock and granulometric fractioning of organic matter in soil use systems in Cerrado. *Revista de Ciências Agrovetenárias* 18, 136–145. <https://doi.org/10.5965/223811711812019136>.
- Nepstad, D.C., Stickler, C.M., Soares-Filho, B., Merry, F., 2008. Interactions Among Amazon Land Use, Forests and Climate: Prospects for a Near-Term Forest Tipping

- Point. Philosophical Transactions of the Royal Society B: Biological Sciences. Royal Society, pp. 1737–1746. <https://doi.org/10.1098/rstb.2007.0036>.
- Norby, R.J., Zak, D.R., 2011. Ecological Lessons from Free-air CO₂ Enrichment (FACE) Experiments. *Annu. Rev. Ecol. Evol. Syst.* 42, 181–203. <https://doi.org/10.1146/annurev-ecolsys-102209-144647>.
- Plant, G., Kort, E.A., Murray, L.T., Maasakkers, J.D., Aben, I., 2022. Evaluating urban methane emissions from space using TROPOMI methane and carbon monoxide observations. *Remote Sens. Environ.* 268, 112756. <https://doi.org/10.1016/j.rse.2021.112756>.
- Rahman, A.F., Gamon, J.A., Fuentes, D.A., Roberts, D.A., Prentiss, D., 2001. Modeling spatially distributed ecosystem flux of boreal forest using hyperspectral indices from AVIRIS imagery. *J. Geophys. Res. Atmos.* 106, 33579–33591. <https://doi.org/10.1029/2001jd900157>.
- Reichstein, M., Bahn, M., Ciais, P., Frank, D., Mahecha, M.D., Seneviratne, S.I., Zscheischler, J., Beer, C., Buchmann, N., Frank, D.C., Papale, D., Rammig, A., Smith, P., Thonicke, K., Van Der Velde, M., Vicca, S., Walz, A., Wattenbach, M., 2013. Climate extremes and the carbon cycle. *Nature*. <https://doi.org/10.1038/nature12350>.
- Rossi, F.S., Santos, G.A. de A., 2020. Fire dynamics in Mato Grosso State, Brazil: the relative roles of gross primary productivity. *Big Earth Data* 4, 23–44. <https://doi.org/10.1080/20964471.2019.1706832>.
- Rossi, F.S., de Araújo Santos, G.A., de Souza Maria, L., Lourençoni, T., Pelissari, T.D., Della-Silva, J.L., Júnior, J.W.O., de Avila e Silva, A., Lima, M., Teodoro, P.E., Teodoro, L.P.R., de Oliveira-Júnior, J.F., La Scala, N., da Silva Junior, C.A., 2022. Carbon dioxide spatial variability and dynamics for contrasting land uses in central Brazil agricultural frontier from remote sensing data. *J South Am Earth Sci* 103809. <https://doi.org/10.1016/j.jsames.2022.103809>.
- Rossi, F.S., La Scala, N., Capristo-Silva, G.F., Della-Silva, J.L., Teodoro, L.P.R., Almeida, G., Tiago, A.V., Teodoro, P.E., Silva, Junior, C A, da, 2023. Implications of CO₂ emissions on the main land and forest uses in the Brazilian Amazon. *Environ. Res.* 227, 115729. <https://doi.org/10.1016/j.envres.2023.115729>.
- Rouse Jr., J.W., Haas, R.H., Schell, J.A., Deering, D.W., 1974. Monitoring vegetation systems in the great Plains with ERTS. In: *Proceeding of ERTS-1 Symposium*, p. 309.
- Running, S.W., Zhao, M., 2015. MOD17A2H MODIS/Terra gross primary productivity 8-day L4 global 500m SIN Grid V006. NASA EOSDIS land processes distributed active Archive center. <https://doi.org/10.5067/MODIS/MOD17A2H.006>.
- Running, S., Mu, Q., Zhao, M., 2015. MOD17A2H MODIS/Terra gross primary productivity 8-day L4 global 500m SIN Grid V006. <https://doi.org/10.5067/MODIS/MOD17A2H.006>.
- Rustogi, P., Landschützer, P., Brune, S., Baehr, J., 2023. The impact of seasonality on the annual air-sea carbon flux and its interannual variability. *NPJ Clim Atmos Sci* 6, 66. <https://doi.org/10.1038/s41612-023-00378-3>.
- Santos, C.V.B. dos, 2017. Modelagem Espectral Para Determinação De Fluxo De Co₂ Em Áreas De Caatinga Preservada E Em Regeneração (Master Thesis). Universidade Estadual de Feira de Santana, Feira de Santana.
- Schwalm, C.R., Anderegg, W.R.L., Michalak, A.M., Fisher, J.B., Biondi, F., Koch, G., Litvak, M., Ogle, K., Shaw, J.D., Wolf, A., Huntzinger, D.N., Schaefer, K., Cook, R., Wei, Y., Fang, Y., Hayes, D., Huang, M., Jain, A., Tian, H., 2017. Global patterns of drought recovery. *Nature* 548, 202–205. <https://doi.org/10.1038/nature23021>.
- Silva, C.A., Lima, M., 2018. Soy moratorium in Mato Grosso: deforestation undermines the agreement. *Land Use Pol.* 71, 540–542. <https://doi.org/10.1016/j.landusepol.2017.11.011>.
- Silva Junior, C.A. da, Leonel-Junior, A.H.S., Rossi, F.S., Filho, W.L.F.C., de Barros Santiago, D., de Oliveira-Júnior, J.F., Teodoro, P.E., Lima, M., Capristo-Silva, G.F., 2020. Mapping soybean planting area in midwest Brazil with remotely sensed images and phenology-based algorithm using the Google Earth Engine platform. *Comput. Electron. Agric.* 169, 105194. <https://doi.org/10.1016/j.compag.2019.105194>.
- Souza, A.P.D., Teodoro, P.E., Teodoro, L.P.R., Taveira, A.C., de Oliveira-Júnior, J.F., Della-Silva, J.L., Baio, F.H.R., Lima, M., da Silva Junior, C.A., 2021. Application of remote sensing in environmental impact assessment: a case study of dam rupture in Brumadinho, Minas Gerais, Brazil. *Environ. Monit. Assess.* 193, 606. <https://doi.org/10.1007/s10661-021-09417-z>.
- Stein, R.A., Keppel-Aleks, G., Levin, N.E., Poulsen, C.J., 2020. Carbon and Water Dynamics in Modern and Ancient Plants and Soils (Dissertation). University of Michigan, Ann Arbor.
- Streher, A.S., Torres, R. da S., Morellato, L.P.C., Silva, T.S.F., 2020. Accuracy and limitations for spectroscopic prediction of leaf traits in seasonally dry tropical environments. *Remote Sens. Environ.* 244, 111828. <https://doi.org/10.1016/j.rse.2020.111828>.
- Upadhyay, S., Raghubanshi, A.S., 2020. Chapter 16 - Determinants of soil carbon dynamics in urban ecosystems. In: Verma, P., Singh, P., Singh, R., Raghubanshi, A.S. (Eds.), *Urban Ecology*. Elsevier, pp. 299–314. <https://doi.org/10.1016/B978-0-12-820730-7.00016-1>.
- Wang, P., Holloway, T., Bindl, M., Harkey, M., De Smedt, I., 2022. Ambient formaldehyde over the United States from ground-based (AQ5) and satellite (OMI) observations. *Remote Sens. (Basel)* 14. <https://doi.org/10.3390/rs14092191>.
- Welp, L.R., Keeling, R.F., Meijer, H.A.J., Bollenbacher, A.F., Piper, S.C., Yoshimura, K., Francey, R.J., Allison, C.E., Wahlen, M., 2011. Interannual variability in the oxygen isotopes of atmospheric CO₂ driven by El Niño. *Nature* 477, 579–582. <https://doi.org/10.1038/nature10421>.
- Wieneke, S., Ahrends, H., Damm, A., Pinto, F., Stadler, A., Rossini, M., Rascher, U., 2016. Airborne based spectroscopy of red and far-red sun-induced chlorophyll fluorescence: Implications for improved estimates of gross primary productivity. *Remote Sens. Environ.* 184, 654–667. <https://doi.org/10.1016/j.rse.2016.07.025>.
- Yao, J., Henderson, S.B., 2014. An empirical model to estimate daily forest fire smoke exposure over a large geographic area using air quality, meteorological, and remote sensing data. *J. Expo. Sci. Environ. Epidemiol.* 24, 328–335. <https://doi.org/10.1038/jes.2013.87>.
- Zeri, M., Oliveira-Júnior, J.F., Lyra, G.B., 2011. Spatiotemporal analysis of particulate matter, sulfur dioxide and carbon monoxide concentrations over the city of Rio de Janeiro, Brazil. *Meteorol. Atmos. Phys.* 113, 139. <https://doi.org/10.1007/s00703-011-0153-9>.
- Zhang, L., Tian, H., Shi, H., Pan, S., Qin, X., Pan, N., Dangal, S.R.S., 2021. Methane emissions from livestock in East Asia during 1961–2019. *Ecosys. Health Sustain.* 7, 1918024. <https://doi.org/10.1080/20964129.2021.1918024>.
- Žížala, D., Minařík, R., Zádorová, T., 2019. Soil organic carbon mapping using Multispectral remote sensing data: prediction Ability of data with different spatial and spectral resolutions. *Remote Sens. (Basel)* 11. <https://doi.org/10.3390/rs11242947>.